A Journal of the Gesellschaft Deutscher Chemiker

Angewandte International Edition

GDCh

Chemie

www.angewandte.org

Accepted Article

Title: In-situ Thermal atomization to Transfer Supported Metal Nanoparticles to Surface Enriched Ni Single atom catalyst

Authors: Jian Yang, Zongyang Qiu, Changming Zhao, Weichen Wei, Wenxing Chen, Zhijun Li, Yunteng Qu, Juncai Dong, Jun Luo, Zhenyu Li, and Yuen Wu

To be cited as: *Angew. Chem. Int. Ed.* 10.1002/anie.201808049
Angew. Chem. 10.1002/ange.201808049

Link to VoR: http://dx.doi.org/10.1002/anie.201808049
http://dx.doi.org/10.1002/ange.201808049

WILEY-VCH

10.1002/anie.201808049

WILEY-VCH

In-situ Thermal atomization to Transfer Supported Metal Nanoparticles to Surface Enriched Ni Single atom catalyst

Dr. Jian Yang,† Dr. Zongyang Qiu,† Dr. Changming Zhao,† Dr. Weichen Wei, Dr. Wenxing Chen, Dr. Zhijun Li, Dr. Yunteng Qu, Prof. Juncai Dong, Prof. Jun Luo, Prof. Zhenyu Li,* Prof. Yuen Wu*

Dedication ((optional))

Abstract: Arrange the active sites on the surface of the catalysts can extremely estimate the problem of mass transfer and enhance the atom economy, which is a primary goal in heterogeneous catalysis. Herein, a unique phenomenon that supported Ni metal nanoparticles can be transformed to thermal stable Ni single atoms, which is mostly located on the surface of the support, has been uncovered. Assisted by the N-doped carbon with abundant defects, this synthetic process not only transform the nanoparticles to single atoms, but also create numerous pores to facilitate the contact of dissolved CO_2 and single Ni sites. The proposed ''Pac-Man'' mechanism is that the Ni nanoparticles could break surface C-C bonds drill into the carbon matrix, leaving abundant pores on the surface. When Ni nanoparticles are exposed to N defects C, the strong coordination would split the Ni atoms from Ni nanoparticles, which would be further stabilized within the surface of carbon substrate. The continuous loss of atomic Ni species from the NPs would finally result in atomization of Ni NPs. CO_2 electroreduction testing shows that the surface enriched Ni single atoms (defined as SE-Ni SAs@PNC) delivers superior performance than supported Ni NPs and other Ni SAs catalysts, with 88% CO formation Faradaic efficiency (FE) and a current density of 18.3 mA/cm^2 at a potential of -1.0 V. Moreover, the CO formation turnover frequency (TOF) reaches a high value of 47805 h^{-1}, which surpasses most of reported metal-based catalysts under comparable conditions.

Due to the massive CO_2 produced by consuming the carbon fuels, a serious of climatic problems have been triggered, especially global warming and glaciers melting.[1] It is critically urgent to search for the efficient ways to decrease the CO_2 accumulation in air. Recently, electroreduction of CO_2 has been regarded as a promising approach to eliminate CO_2 as well as convert to the other useful raw materials, such as CO, CH_4, C_2H_4, HCOOH and so on.[2] The ideal features for CO_2 electroreduction heterogeneous catalyst should contain highly dispersed active species on the support and sufficient accessible surface to remit the problem of the mass transfer. Hence, a porous support is pressingly adopted, which could not only stabilize the reactive sites but also guarantee the fast adsorption of reactants and desorption of products. Recently, single atoms catalysts have drawn much attention toward the electroreduction of CO_2 due to their satisfactory electrochemical performances and excellent atom economy.[3] However, the main problem is the most of the synthetic methods for single atoms catalysts are based on the bottom-up strategy, which the metal ions are adsorbed on the defective matrix and then reduced to form single atoms in the whole support.[4] Based on this bottom-up method, the porous support are incapable to regulate most of the atomic metal species on the surface owing to their powerlessness in remitting the migration of supported metal within the matrix. This will result in the homogeneous distribution of single metal sites within the entire skeleton rather than on the surface, which usually cause the issue of mass transportation and deactive in the catalytic process. To solve this challenge, we describe a novel top-down strategy, during which the Ni NPs distributed on the surface of defective NC support can be transformed into surface enriched Ni single atoms by thermal diffusion mechanism, which is quite different with the previous reports through vaporing the nanoparticles form gas phase intermediate.[5] The Ni NPs could play a part of ''Pac-Man'' to bit off surface C-C bonds. At the same time, when Ni NPs diffuse within the N defective C matrix, the Ni atoms can be bound by the N-rich defects. As a result, Ni NPs are gradually weared and finally transformed into atomic dispersion.[6] This phenomenon is also found in noble metal system.[7]

As illustrated in Figure 1a, we select the NC support with an average diameter of 200 nm obtained by a simple pyrolysis treatment of ZIF-8 (Figure S1) as a support. The uniform Ni NPs with a diameter of approximately 5 nm are firstly prepared by reduction of nickel acetylacetonate (Figure S2).[8] Loading the Ni NPs on the surface of the NC support (Figure 1b), a typical supported metal catalyst by a stirring and centrifugation process (defined as Ni NPs@NC). Careful examinations confirm that the size of supported Ni NPs are typically as same as the initial Ni NPs (Figure 1c and S2). The elemental mapping further reveals homogeneous distribution of Ni NPs on the surface of NC (Figure 1d). In order to convert Ni NPs into atomic dispersive Ni atoms, the supported Ni NPs@NC sample is exposed to a thermal treatment at 1173 K in Ar. As shown in Figure 1e, the external Ni NPs thoroughly disappeared and abundant pores are generated on the surface of NC support. Because of the high melting point and boiling point of Ni (1726 K and 3005 K), the Ni atoms are not likely volatilized away during the thermal process. Aberration corrected high-angle annular dark-field scanning transmission electron microscope (HAADF-STEM) measurement with subangstrom resolution is used to confirm the existence of Ni atoms. The isolated Ni single atoms can be unambiguously discerned on the NC support, exhibiting enrichment at 5-10 nm thick shell near the surface (Figure 1f). Furthermore,

J. Yang, C. Zhao, W. Wei, Z. Li, Y. Qu, Y. Wu
Department of Chemistry, iChEM (Collaborative Innovation Center of Chemistry for Energy Materials), University of Science and Technology of China, Hefei 230026, China
E-mail: yuenwu@ustc.edu.cn; zyli@ustc.edu.cn
Z. Qiu, Z. Li
Hefei National Laboratory for Physical Sciences at the Microscale, University of Science and Technology of China, Hefei 230026, China
W. Chen, J. Dong, J. Luo
Department of Chemistry, Tsinghua University, Beijing 100084 (P. R. China) Beijing Key Laboratory of Construction Tailorable Advanced Functional Materials and Green Application, School of Materials Science and Engineering, Beijing Institute of Technology, Beijing 100081, China; Institute of High Energy Physics Beijing 100029, China; Institute for New Energy Materials & Low-Carbon Technologies, Tianjin University of Technology Tianjin 300384, China
‡ These authors contributed equally.

examination of other areas demonstrates the absence of either Ni nanoparticles or clusters (Figure S3), suggesting the successful evolution from supported Ni NPs to single atoms (SAs). The elemental mapping and EDS (energy dispersive spectroscopy) synergistically confirm the Ni atoms are homogeneously distributed on the surface of the whole NC matrix (Figure 1g and S4). To further demonstrate the surface-enriched Ni single atoms, the XPS (X-ray photoelectron spectroscopy) with the deferent energy receiving angle is adoped (Figure S5). When the angle is equal to 300, the peak intensity is far higher than that of 900, which is revealed that the Ni single atoms are mainly concentrated in the surface of NC support. Meaniwhile, we have also added superfluous Ni NPs solution (200ul and 500ul) on the suface of NC matrix (Figure S6). Unfortunately, due to the limited N defects of NC matrix, these Ni NPs have an obvious agglomeration demonstrating a proper content of Ni NPs on the suface of NC is essential.

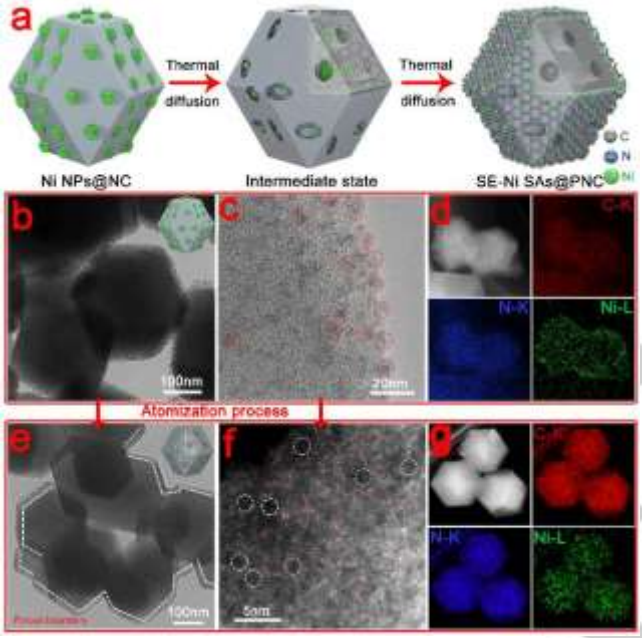

Figure 1. a) Scheme of Ni NPs to Ni SAs transformation and structural characterizations. b) TEM image, c) HRTEM image and d) EDS mapping of Ni NPs@NC. e) TEM image, f) aberration corrected high-angle annular dark-field scanning TEM atomic image and g) EDS mapping of SE-Ni SAs@PNC.

To further confirm the importance of NC support, a control experiment that the Ni NPs are uniformly dispersed on the non-defective XC-72 carbon (defined as Ni NPs@AC) are prepared (Figure S7). As shown in Figure S8, the monodispersity and homogeneity of Ni NPs supported on the XC-72 matrix without any aggregations are clearly discerned. Nevertheless, following a pyrolysis treatment (defined as Ni NPs@C), an obvious aggregation during which the small Ni NPs becomes larger from 5nm to about 50 nm is found (Figure S9), implying a representative Ostwald-ripening process. The high resolution TEM (HRTEM) image shows the large Ni NPs nanocrystallites are embedded on the carbon support, and the specific lattice spacing of (111) facet is measured to be 0.203 nm (Figure S9c). The elemental mapping is employed to confirm the bright plots are designated to the grown Ni NPs, proving the migration and aggregation of Ni atoms cannot be prohibited by the non-defective XC-72 carbon (Figure S9d-f). These results undisputedly demonstrate that the defective NC is a key factor for the transformation of Ni NPs to SAs.

X-ray powder diffraction (XRD) is performed to verify the composition and structural evolution. As exhibited in Figure S10, the NC support shows a poor crystallinity, which coincides well with the previous report that the NC only adopts the short range regular arrangement.[9] SE-Ni SAs@PNC exhibits no characteristic peaks of Ni crystals, whereas the Ni NPs@C sample shows clear peaks of Ni crystal, in line with the aforementioned TEM result. X-ray absorption fine-structure (XAFS) measurement is adopted to characterize the local coordination of Ni samples at the atomic level. As exhibited in the X-ray absorption near-edge structure (XANES) spectra (Figure S11), the position of the white line peak for Ni NPs@C is closer to the position of Ni foil after a heating process, indicating the zero valence state of Ni NPs. In contrast, the position of SE-Ni SAs@PNC locates above the position of Ni foil, demonstrating the partial positive charged Ni SAs. Further structural information for Ni atoms can be obtained from the extended X-ray absorption fine structure (EXAFS) measurement. Before the heating process, the Ni NPs@NC shows a main coordination peak at 2.15 Å (Figure 2a), which can be ascribed to the Ni-Ni path. After a heating process, a dominant peak assigned to the Ni-N coordination at 1.32 Å appears and the corresponding Ni-Ni peak at 2.15 Å disappears for the SE-Ni SAs@PNC. This strongly supports the alteration of local structures of Ni species from the Ni-Ni coordination to Ni-N coordination before and after the thermal atomization process. When the support is replaced by XC-72, a strong peak attributed to the Ni-Ni path is observed and the Ni-N is absent, demonstrating the thermal atomization do not occur over the pure carbon support. Wavelet transform (WT) is adopted to further analyze Ni K-edge EXAFS oscillations. The WT contour plots of SE-Ni SAs@PNC exhibit only one intensity maximum at 4.1 $Å^{-1}$ (Figure 2b), which can be assigned to the Ni-N coordination. No intensity maximum corresponds to Ni-Ni coordination can be observed when compared with the WT plots of Ni foil (Figure S12), also excluding the presence of large Ni clusters and nanoparticles. In contrast, the WT maximums at 6.7 and 6.8 $Å^{-1}$ for Ni NPs@NC (Figure 2c) and Ni NPs@C (Figure 2d) can be both assigned to the Ni-Ni bonding. To obtain the quantitative chemical configuration of Ni atom, quantitative EXAFS fitting is performed to extract the structural parameters (Figure S13 and Table S1). The first shell of the Ni atoms in SE-Ni SAs@PNC exhibits a coordination number of 4.3 and a mean bond length of 1.89 Å, whereas the Ni NPs@NC shows a nearly full coordination number of 12 and a 2.48 Å bond length.

To further confirm the local chemical environments of N element, near edge X-ray absorption fine structure (NEXAFS) and X-ray photoelectron spectroscopy (XPS) is employed (Figure 2e and S14). As shown in Figure 2e, the peaks of A, B, C and D originate from pyridinic, pyrrolic and graphitic N π* and N-C σ* transitions, respectively.[10] Compared to the N K-edge of NC matrix, the relative intensity of π* band decreases compared to that of σ* band for SE-Ni SAs@PNC sample, suggesting a reduction process of C=N bond and the formation of Ni-N coordinate bond once the Ni single atoms are generated.[11] The XPS result further indicates the coexistence of the pyridinic, pyrrolic and graphitic N in the SE-Ni SAs@PNC sample (Figure S14). To demonstrate that the Ni NPs can bit off the C-C bond to create massive pores, the BET specific surface area are calculated by recording N_2 adsorption-desorption isotherms at 77 K (Figure 2f). The BET surface area of SE-Ni SAs@PNC is 1174 m^2/g, which is much higher than that NC sample (943 m^2/g), indicating that a higher amount of pores are created during the thermal atomization process. This result is also consistent with the pore size distribution calculated by HK and BJH methods (Figure 2g and S15). In spite of the identical peak values centering at 0.41 nm, the pore volume for SE-Ni

SAs@PNC (0.44 m^3/g) are much higher than that of NC (0.22 m^3/g), suggesting the newly formation of pores by the migration of Ni NPs into the NC substrate. The larger BET area and more pores are contributed to the higher CO_2 adsorption than that of NC sample, which are in favour of the latter CO_2 reduction catalysis (Figure S16).

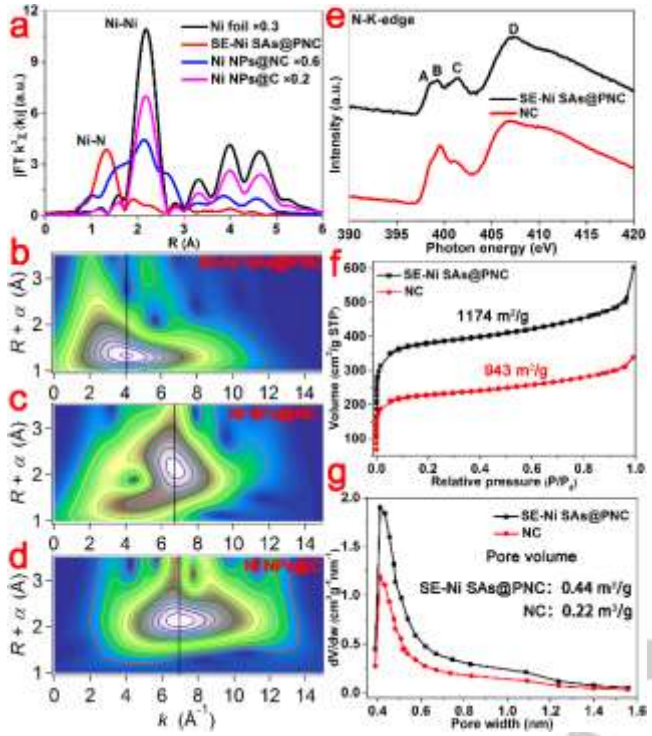

Figure 2. a) FT-EXAFS spectra of Ni foil, SE-Ni SAs@PNC, Ni NPs@NC and Ni NPs@C. WT-EXAFS of b) SE-Ni SAs@PNC, c) Ni NPs@NC and d) Ni NPs@C. e) N K-edge NEXAFS spectra of NC and SE-Ni SAs@PNC. f) N_2 adsorption and desorption isotherm and g) the corresponding pore diameter distribution for SE-Ni SAs@PNC and NC calculated from HK method.

To understand the transformation from Ni NPs to SAs, an environmental TEM is employed to *in-situ* observe this process under Ar atmosphere (supplementary Movie S1). The representative images at different temperatures are exhibited in Figure 3a-f. The average size of Ni NPs on the NC surface is gradually increased from the room temperature to 673 K shown in the TEM images (Figure 3a-c). Meanwhile, when the temperature is further elevated (Figure 3d-f), these Ni NPs are finally vanished, which is demonstrated an obvious aggregation process and further atomization process. The *in-situ* environmental TEM result clearly shows the evolution from Ni NPs to single atoms. Density functional theory based first-principles calculations are performed by VASP package to elucidate the intrinsic evolution mechanism. Single Ni adatom adsorption configurations on N doped and pure graphene are shown in Figure 3g and Figure S17. The most stable adsorption site is the highly symmetrical center of pyrrolic and pyridinic N dopants with binding energies of 6.98 and 7.75 eV, respectively. On pure or quatemary N doped graphene, there are three possible adsorption sites, namely top, bridge and hexagonal center site. On the pure graphene, Ni adatom can adsorb on bridge and hexagonal center site stablely,[12] while the Ni adatom on the top and nearby hexagonal center site of quatemary N are not stable which will be optimized to N-C bridge and the top of para-C site.

Ni dimer's adsorption is more complex which can adsorb parallelly or perpendicularly on graphene plane (Figure S18-21).[13] One kind of perpendicular configurations is that two Ni atoms adsorb on two sides of pyrrolic or pyridinic N dopants equivalently; the other can be regarded as an extra Ni atom adsorption on the stable Ni adatom described above. These configurations' binding energies are about 4.6 eV which are higher than that of parallel configurations. In addition, the binding energies of the extra Ni adatom in the latter perpendicular configurations are smaller than 2.1 eV which indicates the extra Ni adatom is easy to diffuse away. On the pure or quatemary N doped graphene, dimer's binding energies of are about 2.0 eV, lower than that of dimers in pyrrolic and pyridinic N dopants. Besides, the diffusion of dimer on graphene is thought to be easy.[14] So our DFT calculations show that Ni adatom is very stable at pyrrolic and pyridinic N dopants, resulting that Ni atoms are easy to be trapped there and atomically disperse in support.

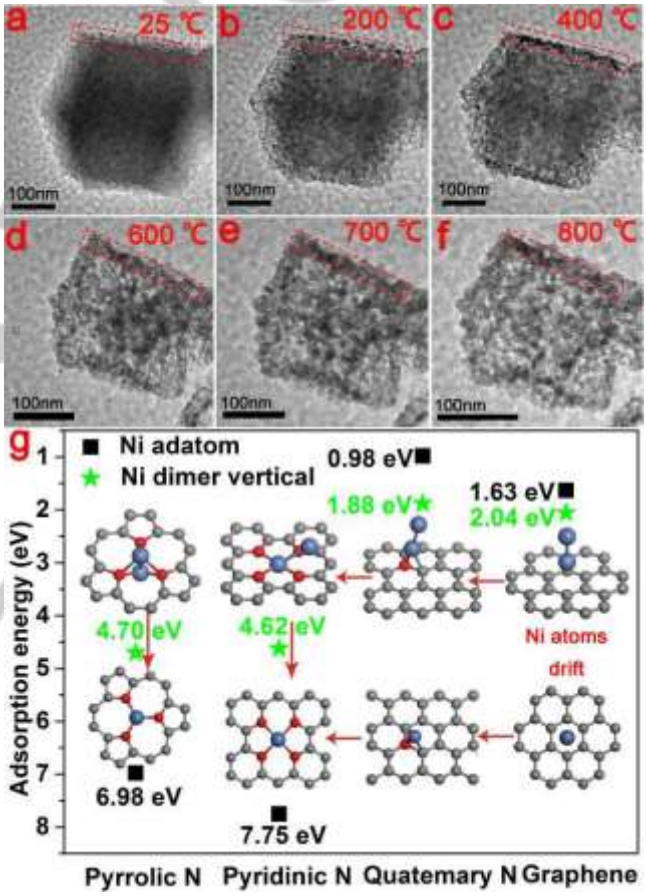

Figure 3. Representative movie images acquired at a) 25℃, b) 200℃, c) 400℃, d) 600℃, e) 700℃ and f) 800℃ of Ni NPs@NC pyrolyzed *in-situ* TEM. g) The adsorption energies of Ni adatom and Ni dimer vertical of pyrrolic N, pyridinic N, quatemary N and graphene. All values are in eV per Ni atom. (Gray, blue and red balls represent C, Ni and N, respectively)

Not only theoretically but also experimentally, it has been confirmed that Ni SAs have high CO_2 electroreduction activity.[15] Hence, the electroreduction of CO_2 of these Ni catalysts, drop-cast onto the 1×1 cm^2 carbon paper, is performed in a standard three–electrode H-cell in 0.5 M $KHCO_3$ solution purging with the excessive CO_2 gas. As shown in Figure 4a and S22, the current density plots at each potential are measured under CO_2-saturated 0.5 M $KHCO_3$ solution. Due to the excellent hydrogen

evolution performance of Ni NPs,[16] Ni NPs@NC and Ni NPs@C electrocatalysts unsurprisingly exhibit a few higher current densities than that of NC and SE-Ni SAs@PNC. Furthermore, the selectivity and activity of electrocatalysts are confirmed by monitoring of the products formed at different potentials collected over 3 h of electrolysis with gas chromatographic (GC) analysis and ^{1}H nuclear magnetic resonance (NMR). The results demonstrate that CO and H_2 are dominant products for the all studied electrocatalysts (Figure 4b, S23). Specifically, the NC and Ni NPs@NC electrocatalysts both only reach FE for CO less than 1% at potentials of -0.7 to -1.2 V (all potentials are referenced to RHE). In contrast, the SE-Ni SAs@PNC sample can achieve over 90% CO and less 10% H_2 (Figure S24) selectivity at the potentials of -0.6 to -1.0 V, revealing that Ni single atoms are the active sites for the CO_2 electroreduction. The CO production TOF normalized to single Ni atoms of SE-Ni SAs@PNC achieves 27898, 47805 and 48842 h^{-1} at the potential of -0.9, -1.0 and -1.1 V, respectively (Figure 4c). Meanwhile, the maximum partial CO current density is up to 16.42 mA/cm^2 at the potential of 1.1 V. As far as we know, taking the potential of 1.0 V at CO_2-saturated 0.5 M $KHCO_3$ solution, such a high current density (18.3 mA/cm^2), CO selectivity (87.8%) and TOF (47805 h^{-1}) index outperforms those of the most of reported electrocatalysts (Table S2). Furthermore, mechanistic insight into the electroreduction of CO_2 to CO on the SE-Ni SAs@PNC can be obtained from the Tafel slope (Figure S25). According to the previous report, the Tafel slope of 151 mV/dec reached by SE-Ni SAs@PNC sample shows a similar value with that of polycrystalline Ag, demonstrating forming CO_2^- intermediate species on the single Ni atoms is the rate-determining step.[17] Moreover, to assess the stability of SE-Ni SAs@PNC, continuous CO_2 electroreduction is carried out at -1.0 V for 60 h. No obvious activity decay and structure change are observed for the durability test of SE-Ni SAs@PNC (Figure 4d, S26), which reveals the robustness of Ni-N active centers over NC support under test conditions. To further judge the impact of spatial distribution of single Ni sites on the support in influencing the catalytic performance, another single atom catalysts with Ni SAs distributing over the entire NC matrix have been synthesized according to previously reported ionic exchange method (defined as Ni SAs@N-C).[3d] As a result, not only the current density (18.3 mA/cm^2 vs. 10.48 mA/cm^2) at -1.0 V, but also the CO FE (88% vs. 70%) delivered by SE-Ni SAs@PNC (18.3 mA/cm^2) is superior to that of Ni SAs@N-C. More importantly, the TOF value at -1.0 V shows 47805 h^{-1} for Ni SAs@PNC, which is almost nine times larger than that of Ni SAs@N-C (5273 h^{-1}). Due to the favorable mass transfer and fast diffusion, the surface enriched Ni single atoms and porous NC support are unambiguously responsible for the higher catalytic activity.

DFT calculations (detailed computational data are shown in the Supporting Information) are carried out to understand the nature of the superior CO_2 electroreduction activity of SE-Ni SAs@PNC. Here, according to Figure 3g result, Ni-4N, Ni-3N and Ni (111) plane three models (Figure 4e) are constructed to represent Ni SAs and Ni NPs catalysts. The reaction free energies of elementary steps and proposed reaction paths are shown in Figure 4f. As we all known, the reduction of CO_2 to COOH* is considered the first electronic step, which the Ni-3N, Ni-4N and Ni (111) models show 0.895, 1.708 and 0.387 eV, respectively. These calculations demonstrate that the Ni NPs have more optimal ΔG in this step. After that, the COOH* species can be effortless to obtain a proton forming a CO* species with a H_2O melecule release for Ni-4N, Ni-3N and Ni (111) models due to the negative ΔG. And the following CO* species will desorpt from the active center of catalyts. However, the Ni (111) plane has exihibited a more positive free energy (ΔG=1.026 eV) than Ni SAs catalyst (Ni-3N ΔG=-0.177 eV and Ni-4N ΔG=-0.824). Therefore, CO desorption step is strictly limited the CO_2 reduction activity for Ni NPs, which reveals that Ni NPs are not suitable for CO_2 reduction. The calculated result is well consistent with that of the experitmental test.

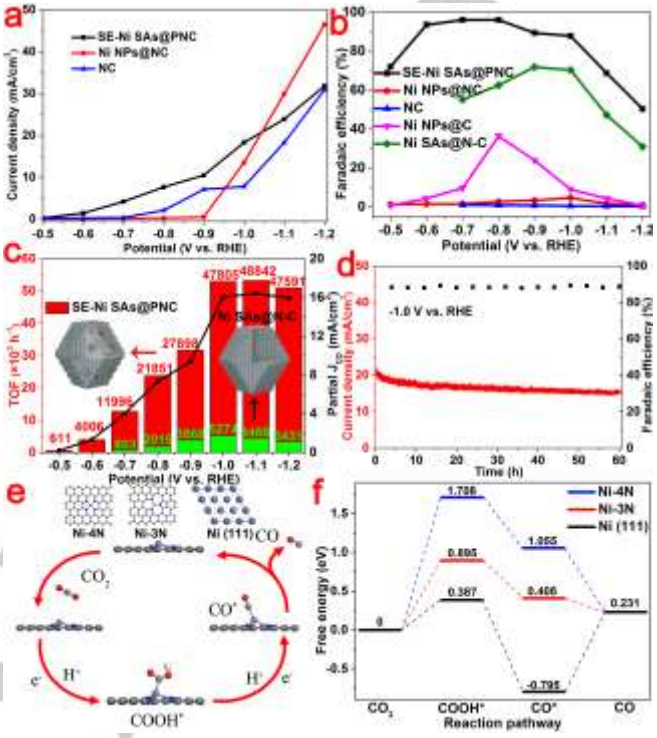

Figure 4. a) The measured current density plots recorded in CO_2-saturated 0.1 M $KHCO_3$ solution under different potentials on SE-Ni SAs@PNC, Ni NPs@NC and NC electrocatalysts. b) FEs of CO at different applied potentials on SE-Ni SAs@PNC, Ni NPs@NC, NC and Ni NPs@C electrocatalysts. c) TOFs, partial CO current density plots and d) Stability of SE-Ni SAs@PNC at a potential of -1.0 V vs. RHE. e) Structural evolution of the active site in electrochemical CO_2 reduction. f) Free energy diagram for the conversion of CO_2 to CO at U=0 V vs. RHE on the SE-Ni SAs@PNC and Ni NPs (111).

In summary, a surface enriched Ni single atoms on the porous NC support catalyst has been successfully synthesized by a ''Pac-Man'' induced thermal atomization. Compared to the Ni single atoms distributed on the whole matrix, surface enriched Ni single atoms on the porous NC support shows favorable mass transfer for CO_2 electroreduction, delivering excellent activity, selectivity and stability. Our findings can provide a new opportunity to synthesize the surface enriched single atoms for further improving the atom utilization.

Acknowledgements

This work was supported by National Key R&D Program of China 2017YFA (0208300) and (0700100), the National Natural Science Foundation of China (21522107, 21671180, 21521091, U1463202). We thank the photoemission endstations BL1W1B in Beijing Synchrotron Radiation Facility (BSRF), BL14W1 in Shanghai Synchrotron Radiation Facility (SSRF), BL10B and BL11U in National Synchrotron Radiation Laboratory (NSRL) for the help in characterizations.

Keywords: Thermal atomization, Ni single atoms, CO_2 electroreduction.

[1] a) J. L. Qiao, Y. Y. Liu, F. Hong, J. Zhang, *J. Chem. Soc. Rev.* **2014**, *43*, 631-675. b) C. W. Li, J. Ciston, M. W. Kanan, *Nature* **2014**, *508*, 504-507.

[2] a) Q. Li, J. J. Fu, W. L. Zhu, Z. Z. Chen, B. Shen, L. H. Wu, Z. Xi, T. Y. Wang, G. Lu, J. J. Zhu, S. H. Sun, *J. Am. Chem. Soc.* **2017**, *139*, 4290-4293. b) S. Gao, Y. Lin, X. C. Jiao, Y. F. Sun, Q. Q. Luo, W. H. Zhang, D. Q. Li, J. L. Yang, Y. Xie, *Nature* **2016**, *529*, 68-71. c) C. T. Dinh, T. Burdyny, M. G. Kibria, A. Seifitokaldani, C. M. Gabardo, F. P. G. de Arquer, A. Kiani, J. P. Edwards, P. De Luna, O. S. Bushuyev, C. Q. Zou, R. Quintero-Bermudez, Y. J. Pang, D. Sinton, E. H. Sargent, *Science* **2018**, *360*, 783-787. d) F. C. Lei, W. Liu, Y. F. Sun, J. Q. Xu, K. T. Liu, L. Liang, T. Yao, B. C. Pan, S. Q. Wei, Y. Xie, *Nat. Commun.* **2016**, *7,* 12697-12705. e) P. P. Su, W. B. Xu, Y. L. Qiu, T. T. Zhang, X. F. Li, H. M. Zhang, *Chemsuschem* **2018**, *11*, 848-853. f) N. Han, Y. Wang, H. Yang, J. Deng, J. H. Wu, Y. F. Li, Y. G. Li, *Nat. Commun.* **2018**, *9,* 1320-1328. g) X. J. Liu, H. Yang, J. He, H. X. Liu, L. D. Song, L. Li, J. Luo, *Small* **2018**, *14,* 1704049-1704056.

[3] a) H. B. Yang, S. F. Hung, S. Liu, K. D. Yuan, S. Miao, L. P. Zhang, X. Huang, H. Y. Wang, W. Z. Cai, R. Chen, J. J. Gao, X. F. Yang, W. Chen, Y. Q. Huang, H. M. Chen, C. M. Li, T. Zhang, B. Liu, *Nat. Energy* **2018**, *3*, 140-147. b) X. Q. Wang, Z. Chen, X. Y. Zhao, T. Yao, W. X. Chen, R. You, C. M. Zhao, G. Wu, J. Wang, W. X. Huang, J. L. Yang, X. Hong, S. Q. Wei, Y. Wu, Y. D. Li, *Angew. Chem. Int. Ed.* **2018**, *57*, 1944-1948. c) Y. Cheng, S. Y. Zhao, B. Johannessen, J. P. Veder, M. Saunders, M. R. Rowles, M. Cheng, C. Liu, M. F. Chisholm, R. De Marco, H. M. Cheng, S. Z. Yang, S. P. Jiang, *Adv. Mater.* **2018**, *30,* 1706287-1706294. d) C. M. Zhao, X. Y. Dai, T. Yao, W. X. Chen, X. Q. Wang, J. Wang, J. Yang, S. Q. Wei, Y. E. Wu, Y. D. Li, *J. Am. Chem. Soc.* **2017**, *139*, 8078-8081. e) X. G. Li, W. T. Bi, M. L. Chen, Y. X. Sun, H. X. Ju, W. S. Yan, J. F. Zhu, X. J. Wu, W. S. Chu, C. Z. Wu, Y. Xie, *J. Am. Chem. Soc.* **2017**, *139*, 14889-14892.

[4] a) L. B. Wang, H. L. Li, W. B. Zhang, X. Zhao, J. X. Qiu, A. W. Li, X. S. Zheng, Z. P. Hu, R. Si, J. Zeng, *Angew. Chem. Int. Ed.* **2017**, *56*, 4712-4718. b) R. Lang, T. B. Li, D. Matsumura, S. Miao, Y. J. Ren, Y. T. Cui, Y. Tan, B. T. Qiao, L. Li, A. Q. Wang, X. D. Wang, T. Zhang, *Angew. Chem. Int. Ed.* **2016**, *55*, 16054-16058. c) W. Liu, L. L. Cao, W. R. Cheng, Y. J. Cao, X. K. Liu, W. Zhang, X. L. Mou, L. L. Jin, X. S. Zheng, W. Che, Q. H. Liu, T. Yao, S. Q. Wei, *Angew. Chem. Int. Ed.* **2017**, *56*, 9312-9317. d) X. F. Yang, A. Q. Wang, B. T. Qiao, J. Li, J. Y. Liu, T. Zhang, *Acc. Chem. Res.* **2013**, *46*, 1740-1748. e) B. T. Qiao, A. Q. Wang, X. F. Yang, L. F. Allard, Z. Jiang, Y. T. Cui, J. Y. Liu, J. Li, T. Zhang, *Nat. Chem.* **2011,** *3*, 634-641. f) A. J. Therrien, A. J. R. Hensley, M. D. Marcinkowski, R. Q. Zhang, F. R. Lucci, B. I. Coughlin, A. C. Schilling, J. S. McEwen, E. C. H. Sykes, *Nat. Catal.* **2018,** *1*, 192-198.

[5] a) L. Nie, D. H. Mei, H. F. Xiong, B. Peng, Z. B. Ren, X. I. P. Hernandez, A. DeLaRiva, M. Wang, M. H. Engelhard, L. Kovarik, A. K. Datye, Y. Wang, *Science*, **2017**, *358*, 1419-1423. b) Z. W. Huang, X. Gu, Q. Q. Cao, P. P. Hu, J. M. Hao, J. H. Li, X. F. Tang, *Angew. Chem. Int. Ed.* **2012,** *51*, 4198-4203. c) R. Bliem, R. Kosak, L. Perneczky, Z. Novotny, O. Gamba, D. Fobes, Z. Q. Mao, M. Schmid, P. Blaha, U. Diebold, G. S. Parkinson, *Acs Nano* **2014**,*8*, 7531-7537.

[6] Z. Y. Qiu, L. Song, J. Zhao, Z. Y. Li, J. L. Yang, *Angew. Chem. Int. Ed.* **2016**, *55*, 9918-9921.

[7] S. J. Wei, A. Li, J. C. Liu, Z. Li, W. X. Chen, Y. Gong, Q. H. Zhang, W. C. Cheong, Y. Wang, L. R. Zheng, H. Xiao, C. Chen, D. S. Wang, Q. Peng, L. Gu, X. D. Han, J. Li, Y. D. Li, *Nat. Nanotech.* **2018**, *13*, 856-861.

[8] O. Metin, V. Mazumder, S. Ozkar, S. S. Sun, *J. Am. Chem. Soc.* **2010**, *132*, 1468-1469.

[9] a) J. Yang, D. S. He, W. X. Chen, W. Zhu, H. Zhang, S. Ren, X. Wang, Q. H. Yang, Y. Wu, Y. D. Li, *Acs Appl. Mater. Inter.* **2017**, *9*, 39450-39455. b) P. Q. Yin, T. Yao, Y. Wu, L. R. Zheng, Y. Lin, W. Liu, H. X. Ju, J. F. Zhu, X. Hong, Z. X. Deng, G. Zhou, S. Q. Wei, Y. D. Li, *Angew. Chem. Int. Ed.* **2016**, *55*, 10800-10805.

[10] X. Wang, W. X. Chen, L. Zhang, T. Yao, W. Liu, Y. Lin, H. X. Ju, J. C. Dong, L. R. Zheng, W. S. Yan, X. S. Zheng, Z. J. Li, X. Q. Wang, J. Yang, D. S. He, Y. Wang, Z. X. Deng, Y. E. Wu, Y. D. Li, *J. Am. Chem. Soc.* **2017**, *139*, 9419-9422.

[11] J. Wang, Z. Q. Huang, W. Liu, C. R. Chang, H. L. Tang, Z. J. Li, W. X. Chen, C. J. Jia, T. Yao, S. Q. Wei, Y. E Wu, Y. D. Li, *J. Am. Chem. Soc.* **2017**, *139*, 17281-17284.

[12] a) T. O. Wehling, A. I. Lichtenstein, M. I. Katsnelson, *Phys. Rev. B* **2011**, *84,* 195414-195421. b) H. Johll, H. C. Kang, E. S. Tok, *Phys. Rev. B* **2009**, *79,* 245416-245434.

[13] C. Cao, M. Wu, J. Z. Jiang, H. P. Cheng, *Phys. Rev. B* **2010**, *81,* 205424-205433.

[14] W. Gao, J. E. Mueller, J. Anton, Q. Jiang, T. Jacob, *Angew. Chem. Int. Ed.* **2013**, *52*, 14237-14241.

[15] a) K. Jiang, S. Siahrostami, T. T. Zheng, Y. F. Hu, S. Hwang, E. Stavitski, Y. D. Peng, J. Dynes, M. Gangisetty, D. Su, K. Attenkofer, H. T. Wang, *Energy Environ. Sci.* **2018**, *11*, 893-903. b) W. Ju, A. Bagger, G. P. Hao, A. S. Varela, I. Sinev, V. Bon, B. R. Cuenya, S. Kaskel, J. Rossmeisl, P. Strasser, *Nat. Commun.* **2017**, *8*, 944-953. c) K. Jiang, S. Siahrostami, A. J. Akey, Y. B. Li, Z. Y. Lu, J. Lattimer, Y. F. Hu, C. Stokes, M. Gangishetty, G. X. Chen, Y. W. Zhou, W. Hill, W. B. Cai, D. Bell, K. Chan, J. K. Norskov, Y. Cui, H. T. Wang, *Chem* **2017**, *3*, 950-960. d) K. Jiang, G. X. Chen, H. T. Wang, Jove-J. Vis. Exp. 2018, 134, e57380-57387.

[16] S. J. Gutic, A. S. Dobrota, M. Leetmaa, N. V. Skorodumova, S. V. Mentus, I. A. Pasti, *Phys. Chem. Chem. Phys.* **2017**, *19*, 13281-13293.

[17] Q. Lu, J. Rosen, Y. Zhou, G. S. Hutchings, Y. C. Kimmel, J. G. G. Chen, F. Jiao, *Nat. Commun.* **2014**, *5,* 3242-3248.

10.1002/anie.201808049

WILEY-VCH

We report a novel top-down strategy, during which the Ni NPs distributed on the surface of defective NC support can be transformed into surface enriched Ni single atoms by thermal diffusion mechanism, which is quite different with the previous reports through vaporing the nanoparticles form gas phase intermediate. The Ni NPs could play a part of ''Pac-Man'' to bit off surface C-C bonds. At the same time, when Ni NPs diffuse within the N defective C matrix, the Ni atoms can be bound by the N-rich defects. As a result, Ni NPs are gradually weared and finally transformed into atomic dispersion. CO_2 electroreduction testing shows that the surface enriched Ni single atoms delivers superior performance than supported Ni NPs and other Ni SAs catalysts, with 88% CO formation Faradaic efficiency (FE) and a current density of 18.3 mA/cm^2 at a potential of -1.0 V. Moreover, the CO formation turnover frequency (TOF) reaches a high value of 47805 h^{-1}, which surpasses most of reported metal-based catalysts under comparable conditions.

*Author(s), Corresponding Author(s)**

Jian Yang,† Zongyang Qiu,† Changming Zhao,† Weichen Wei, Wenxing Chen, Zhijun Li, Yunteng Qu, Juncai Dong, Jun Luo, Zhenyu Li, Yuen Wu**

Page No. – Page No.

In-situ Thermal atomization to Transfer Supported Metal Nanoparticles to Surface Enriched Ni Single atom catalyst